processes

MDPI

Article

Stress Prediction Processes of Metal Pressure-Bearing Complex Components in Thermal Power Plants Based on Machine Learning

Shutao Wang [1], Renqiang Shi [1], Jian Wu [2], Yunfei Ma [2], Chao Yang [1] and Huan Liu [2,*]

[1] Jiangsu Frontier Electric Power Technology Co., Ltd., Nanjing 211100, China; wst0806@126.com (S.W.); srq1033126900@163.com (R.S.); yangchao-666666@163.com (C.Y.)
[2] College of Materials Science and Engineering, Hohai University, Changzhou 213200, China; 221608010044@hhu.edu.cn (J.W.); myf2557@126.com (Y.M.)
* Correspondence: liuhuanseu@hhu.edu.cn

Abstract: The real-time stress assessment of metal pressure components is one of the key factors in ensuring the safe operation of thermal power plants. To address the challenge of real-time prediction of stress in the key areas of complex special-shaped metal pressure-bearing components in a certain domestic 300 MW thermal power plant, three typical complex metal pressure-bearing components, the main steam pipe tee (MSPT), the steam drum downcomer joint (DDJ) and the header ligament (HL), were taken as research objects. The stress distribution of the three complex metal pressure-bearing components under different conditions was analyzed through the finite element method, and the stress results at the dangerous points were used as samples to establish training sample data. Subsequently, different machine learning methods were employed to train the sample data. The training results indicate that neural networks (NNs) and the Auto-Sklearn Regression (ASR) models can accurately predict the stress of the key parts of complex metal pressure-bearing components in real time. The ASR method demonstrates better performance in stress prediction of the main steam pipe tee, with a prediction accuracy of ≥96%. The NN model shows better prediction for the header ligament, with a prediction accuracy of ≥94%. These research findings provide effective support for the high-temperature lifespan assessment and safe operation of thermal power plants.

Keywords: thermal power plant; metal pressure component; finite element analysis; machine learning; high-temperature stress prediction

check for updates

Academic Editor: Massimo Caruso

Received: 11 December 2024
Revised: 18 January 2025
Accepted: 27 January 2025
Published: 27 January 2025

Citation: Wang, S.; Shi, R.; Wu, J.; Ma, Y.; Yang, C.; Liu, H. Stress Prediction Processes of Metal Pressure-Bearing Complex Components in Thermal Power Plants Based on Machine Learning. *Processes* **2025**, *13*, 358. https://doi.org/10.3390/pr13020358

Copyright: © 2025 by the authors. Licensee MDPI, Basel, Switzerland. This article is an open access article distributed under the terms and conditions of the Creative Commons Attribution (CC BY) license (https://creativecommons.org/licenses/by/4.0/).

1. Introduction

Given the extensive application of thermal power plants in the energy field, boilers, as one of their core components, have been in operation for a long time under extreme working environments such as high temperature, high pressure, and corrosion. Consequently, an accurate assessment of the boiler's lifespan is of particular significance [1,2]. Within the boiler structure, irregularly shaped key pressure-bearing metal components, such as the main steam pipe tee, the steam drum downcomer joint and the header ligament, due to their non-standard shapes and structures, render it difficult for traditional theoretical calculation formulas to accurately depict their complex stress distribution [3]. The common monitoring approaches for metal components primarily encompass thermal infrared imaging, electrochemical corrosion monitoring, acoustic emission detection, vibration monitoring, and non-destructive testing. However, the limitations of these methods lie in their inability

to provide real-time and accurate stress data. At the same time, these methods may require downtime for maintenance, increasing the operating costs of power plants. Therefore, in order to comprehensively understand and effectively manage the performance of these key metal components, it is urgently necessary to establish a rapid and effective stress analysis and prediction method to provide the effective data support requisite for the assessment of the boiler's lifespan.

In the industrial domain, there are currently two primary approaches for stress prediction of key pressure-bearing components of boilers: the analytical method [4] and the finite element analysis (FEA) method [5]. The analytical method is employed to directly compute the stress distribution of simple structures through mathematical formulas and theoretical models, and has been applied in the R5 integrity assessment program in the UK [6] and the ASME Boiler and Pressure Vessel Code (NH) [7]. In comparison with the analytical method, the FEA method is applicable to the stress analysis of complex-structured metal components, and thus has received extensive applications and research. Relevant studies have shown that FEA can efficiently reveal the stress distribution characteristics of complex metal structures under various working conditions [8]. For example, in the case of typical pressure-bearing components such as pressure vessels and pipelines, FEA not only accurately identifies stress concentration regions and potential failure points but also achieves high-precision residual stress predictions when combined with experimental results [9–11]. These studies have further explored the thermo-mechanical coupling behavior of materials, the impact of corrosion damage, and the influence of local thinning on the safety of components. Additionally, by incorporating reliability analysis methods such as Monte Carlo simulations and the FORM reliability assessment, FEA modeling effectively quantifies the failure probability and lifespan prediction of structures [12], thereby providing guidance for the maintenance and optimization of critical components. Some studies have also integrated FEA with advanced failure criteria or optimization algorithms [13], enhancing the evaluation accuracy of the load-bearing capacity of complex structures and identifying key influencing factors under thermo-mechanical loading or startup conditions. Despite the significant progress in improving precision and comprehensiveness, challenges remain in achieving real-time online predictions for complex irregular metal components while ensuring computational efficiency. This issue is particularly pronounced in thermal power plant boilers, where critical pressure-bearing components often exhibit complex geometries and operate under variable working conditions. Traditional FEA methods face limitations in real-time monitoring and rapid computation. Therefore, maintaining prediction accuracy while improving computational efficiency remains a pressing issue in this field.

In recent years, machine learning and artificial intelligence have witnessed extensive applications in the industrial domain. Bolandi et al. [14] proposed a convolutional neural network (CNN) model that combines physical constraints by embedding a custom loss function based on the stress concentration physical equation to accurately predict the Von Mises stress distribution of damaged steel plates. A total of 61,440 complex samples were generated using the PDE toolbox in MATLAB for training, and the test results indicated that the model could effectively capture the stress concentration at the crack tip, locate the damage region, and achieve better prediction accuracy than traditional mean square error (MSE) models, with an average absolute error of 0.22% and a peak error of 1.5%, providing an efficient method for quickly predicting complex stress distributions. Croom et al. [15] employed a U-Net model founded on convolutional neural networks to rapidly predict the stress distribution in the defective areas of additively manufactured metal microstructures. They trained the model with 100,000 stress data generated by high-resolution FFT-FE, and the U-Net was capable of accurately capturing the stress concentration in complex defects. The computational speed and prediction performance of the model were significantly supe-

rior to those of low-resolution FFT-FE and other CNN models. Similarly, Xiang et al. [16] demonstrated the potent integration of machine learning with advanced synchrotron X-ray techniques for real-time phase segmentation and analysis in recycled aluminum alloys. By leveraging machine learning-enabled phase segmentation strategies, their research elucidated the dynamic nucleation, growth, and interplay of Fe-rich intermetallic phases during solidification. This work not only revealed intricate phase transformations but also highlighted the benefits of applying ultrasonic processing, which reduced the size of α-Al dendrites and intermetallic phases significantly, providing a green and effective strategy for recycled alloy processing. Moreover, Mathew et al. [17] investigated the performance of artificial neural networks (ANNs) and adaptive neuro-fuzzy inference systems (ANFIS) in predicting welding residual stresses, with a focus on the disparities in statistical indicators and prediction accuracy. The outcomes demonstrated that the ANFIS model optimized by a hybrid algorithm surpassed the ANN model trained with the Levenberg–Marquardt algorithm, particularly in the prediction of axial residual stresses. By contrast, the ANN model presented a notable underestimation issue in predicting high stresses. The ANFIS model possesses stronger local interpolation capabilities and is capable of capturing the nonlinear distribution patterns of residual stresses, rendering it more appropriate for complex welding stress analysis. The above research demonstrated that the potent capabilities of machine learning in learning, analysis, and prediction might offer novel prospects for the real-time monitoring of boilers in thermal power plant units. By means of machine learning approaches, it is expected that while ensuring the accuracy of monitoring, the calculation time can be significantly reduced, facilitating faster responses and decision-making in emergent situations and offering more efficient support for the operation of power plants.

Therefore, in this paper, a stress prediction method for the key pressure-bearing irregular metal components of thermal power plants was proposed based on the combination of finite element and machine learning methods. In view of the high-precision advantage of the FEA method in stress calculation, the ANSYS 2022R1 software was used to calculate the static coupled stress distribution of the irregular metal pressure-bearing components of the thermal power plants, and the maximum principal stress values at the dangerous points corresponding to the temperature and internal pressure were obtained. Finally, a machine learning sample library was established, and the rapid stress prediction of the irregular metal pressure-bearing components was then realized through extensive data training.

2. Materials and Methods

2.1. Models for FEA

FEA was performed firstly for obtaining the training data. Three irregularly shaped metal pressure-bearing components of a domestic 300 MW thermal power plant, including the main steam pipe tee (MSPT), the steam drum downcomer joint (DDJ) and the header ligament (HL) were investigated. The material of the studied components is 12Cr1MoV, and its physical properties at different temperatures are presented in Table 1 (which can be found in the China National Standard GB/T 16507.2-2022 [18], Water Tube Boilers Part 2: Materials [S]). The FEA was performed on the ANSYS workbench to determine the stress distribution.

Table 1. The physical properties of 12Cr1MoV at different temperatures.

Temperature (°C)	Density (kg/m^3)	Coefficient of Thermal Expansion (K^{-1})	Young's Modulus (Pa)	Poisson Ratio	Thermal Conductivity (W/(m·K))
20	7860	1.08×10^{-5}	2.14×10^{11}	0.29	45.2
100		1.30×10^{-5}	2.11×10^{11}	0.29	45.2
200		1.34×10^{-5}	2.06×10^{11}	0.29	45.2
300		1.36×10^{-5}	1.95×10^{11}	0.3	42.7
400		1.38×10^{-5}	1.87×10^{11}	0.3	40.5
500		1.42×10^{-5}	1.79×10^{11}	0.3	37.7
600		1.44×10^{-5}	1.67×10^{11}	0.32	35.5

Tetrahedral mesh was used for meshing. Since the special-shaped components are subjected to high temperatures and internal pressures during service, the meshes in the connection transition regions were appropriately refined and densified. The MSPT was divided into 784,907 elements and 1,078,834 nodes, the DDJ was divided into 48,070 elements and 73,207 nodes, and the HL was divided into 93,109 elements and 144,269 nodes. The mesh is illustrated in Figure 1.

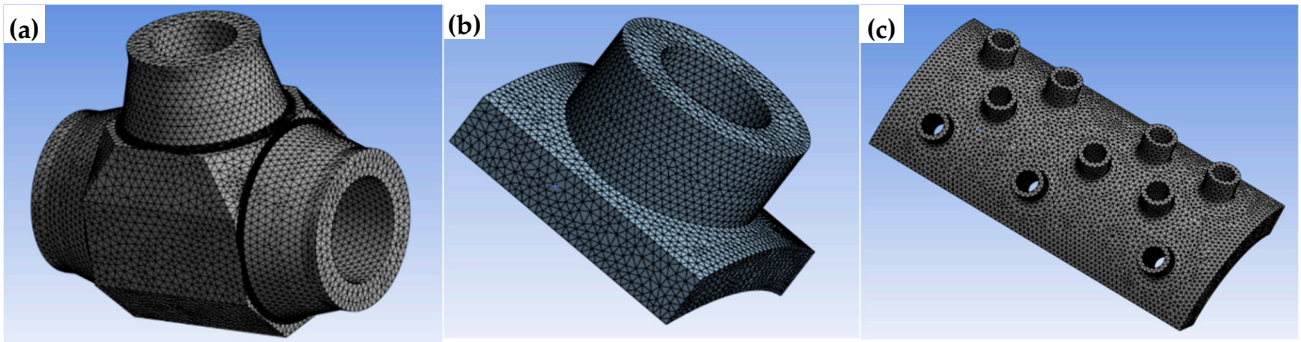


Figure 1. Mesh division diagram of the metal pressure-bearing components with special shapes: (**a**) MSPT; (**b**) DDJ; (**c**) HL.

2.2. Boundary Condition for FEA

Since the pressure-bearing components operate under the coupled effects of high temperature and high pressure, this study adopts a unidirectional thermo-mechanical coupling analysis method, with calculations performed using the indirect method in ANSYS 2022R1 software. The unidirectional coupling approach considers the influence of temperature on structural deformation but neglects the impact of structural deformation on the temperature field, ensuring high computational efficiency and suitability for engineering applications. The specific analysis process involves first conducting a thermal analysis of the structure based on the specified thermal boundary conditions, followed by applying the thermal analysis results as loads in the subsequent structural analysis to obtain the coupled analysis results.

The coupling results satisfy the following equations:

Physical equation:

$$\sigma_{ij} = 2G\varepsilon_{ij} + (A_e - \beta_T)\delta_{ij}$$

Equilibrium equation:

$$\nabla^2 \mathrm{u}_i + \frac{1}{1-2\mu}\frac{\partial \varepsilon_{kk}}{\partial i} - \frac{2(1+\mu)}{1-2\mu}\frac{\partial T}{\partial i} + \frac{f_i}{G} = 0$$

Compatibility equation:

$$\nabla^2\delta_i + \frac{1}{1+\mu}\frac{\partial^2\delta_{kk}}{\partial i^2} = -\alpha_E\left(\frac{1}{1-\mu}\nabla^2 T + \frac{1}{1+\mu}\frac{\partial^2 T}{\partial i^2}\right) - \left(\frac{\mu}{1-\mu}\frac{\partial f_i}{\partial i} + 2\frac{\partial f_i}{\partial i}\right)$$
$$i = j = x, y, z$$

$$\nabla^2\delta_{ij} + \frac{1}{1+\mu}\frac{\partial^2\delta_{kk}}{\partial i\partial j} = -\frac{\alpha_E}{1+\mu}\frac{\partial^2 T}{\partial i\partial j} - \left(\frac{\partial f_i}{\partial j} + \frac{\partial f_j}{\partial i}\right)$$
$$i = x, y, z;\ j = x, y, z,\ and,\ i \neq j$$

In this formula, $\beta = \frac{\alpha_E}{1-2\mu} = \lambda\alpha_E + 2G$, $G = \frac{E}{2(1+\mu)}$, $A = \frac{\mu E}{(1+\mu)(1-2\mu)}$, $\delta_{kk} = \delta_{xx} + \delta_{yy}$, $\varepsilon_{kk} = e = \varepsilon_{xx} + \varepsilon_{yy} + \varepsilon_{zz}$, E represents the elastic modulus, α denotes the coefficient of thermal expansion, μ is the Poisson's ratio, and $f_i(i = x, y, z)$ refers to the components of the unit body force along the coordinate axes.

Based on the actual operating conditions of the boiler, the boundary conditions for the finite element analysis are treated as follows:

- A simplified one-half model is adopted and symmetrical planes are set to enhance the calculation speed.
- The operating pressure is applied to the inner surface of the pressure-bearing component.
- For the thermal boundary, the inner surface is set to the operating temperature, while the outer surface accounts for convective heat transfer.
- The constraints are applied as remote displacement constraints.

In order to ensure the accuracy of the applied FEA parameters, a set of regular components was firstly investigated using the applied FEA parameters. The results of FEA fit well with those calculated through empirical formulas, confirming the reliability of the applied FEA. Additionally, a similar study by Hazizi K et al. [8] also showed a high degree of agreement between FEA and ASME code calculations to evaluate the stress distribution of a vertical pressure vessel. Therefore, the applied FEA could be used to study the stress distribution of the complex components.

Figure 2 presents the typical startup condition data of the final superheater of the thermal power plant. Distinct from the steady-state operation and deep peak shaving conditions, the temperature and internal pressure in the startup condition change significantly over time. Therefore, it contains different real working condition parameters.

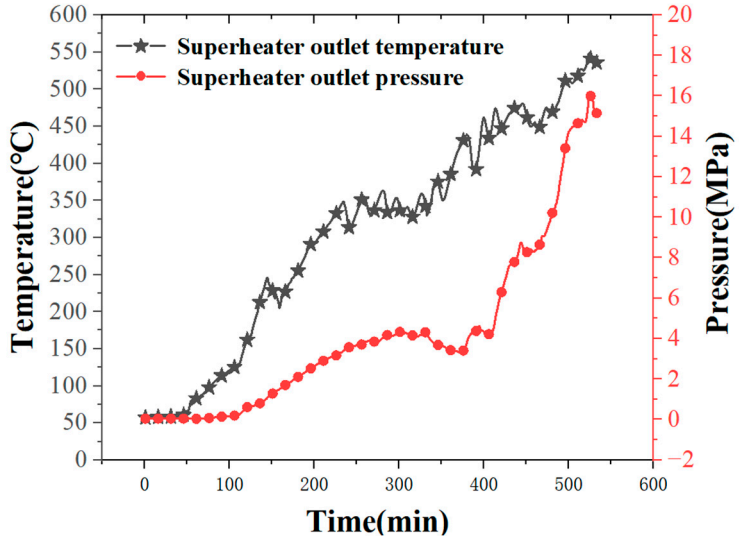


Figure 2. The typical startup condition data of the final superheater in a thermal power plant.

2.3. Model Construction for Machine Learning

Machine learning encompasses multiple disciplines such as computer science, mathematics, and statistics. It is a computer theory developed by allowing computers to learn patterns and regularities from data to fulfill specific tasks. It is mainly classified into four major categories: supervised learning, unsupervised learning, reinforcement learning, and deep learning [19]. In addressing the issue of stress prediction for special-shaped metal pressure-bearing components, this study adopts the supervised learning approach to enhance the efficiency of stress prediction. A variety of machine learning models are attempted, and the accuracy of predictions made by different models is compared. These models comprise the K-nearest neighbors (KNNs), random forests (RFs), neural networks (NNs), gradient boosting regression (GBR), and the Auto-Sklearn Regression (ASR) models, and the model principles are depicted in Figure 3. By conducting training and learning on the above models and adjusting key parameters, the accuracy of these models in predicting stress for irregular metal parts was then evaluated.

(1) KNN model (Figure 3a): it is an instance-based non-parametric learning method, the basic principle of which is to infer the output of an unknown sample by employing the distance measure between points in the sample space. In the regression task, KNNs generate a prediction value by identifying the K nearest neighbors of the target sample in the feature space based on the average or weighted average of its target values among the K nearest neighbors in the training set. Since KNNs do not entail an explicit training process, their model implementation is straightforward and possesses good interpretability, especially in small-scale datasets with uniform sample distribution and low noise.

(2) RF model (Figure 3b): this is an ensemble learning model founded on the bagging concept. By randomly sampling multiple subsets from the original training set and constructing a decision tree on each subset, random forests constitute a regression model composed of numerous decision trees. Each decision tree generates a split point by randomly selecting a subset of input features to mitigate the overfitting risk induced by feature correlation. The ultimate prediction outcome is either the average or the weighted average of all decision tree outputs. The RF model exhibits strong robustness and is capable of handling nonlinear features and noisy data. It inherently supports the evaluation of feature importance.

(3) NN model (Figure 3c): this is a highly flexible and potent nonlinear modeling instrument. Neural networks acquire the complex mapping relationship between input features and target outputs by emulating the connections among biological neurons. The model structure encompasses an input layer, a hidden layer, and an output layer, with neurons in each layer being interconnected by weights and biases. The information flow is processed through differentiable nonlinear activation functions such as ReLU or Sigmoid. During the model training procedure, the backpropagation algorithm is employed to compute the gradient of the loss function, and the gradient descent method is utilized to optimize network parameters, thereby gradually reducing the prediction error. In regression tasks, neural networks are capable of capturing highly intricate nonlinear relationships, rendering them appropriate for modeling physical systems with complex stress field distributions.

(4) GBR model (Figure 3d): it is a gradient-boosting decision tree model based on the concept of incremental ensemble learning via boosting. Its core principle resides in constructing multiple weak learners (typically shallow decision trees) through iterative training. In every round of training, each new decision tree focuses on fitting the residuals of the previous model, thereby continuously enhancing the overall prediction performance. Unlike the parallel training strategy of random forests, GBR adopts a serial training approach, where weak learners possess a sequential and dependent relationship, enabling it to better capture the subtle patterns in the data. GBR performs outstandingly in nonlinear

regression tasks, particularly for medium-sized and small-sized datasets with complex features and moderate noise.

(5) ASR model (Figure 3e): it is an integrated regression model founded on the framework of automated machine learning (AutoML) [20], aimed at enhancing modeling efficiency and prediction accuracy through the automation of hyperparameter optimization and algorithm selection. The core components of ASR comprise a model search engine based on Bayesian optimization, automatic feature preprocessing strategies, and a final model combination founded on ensemble learning. In contrast to traditional machine learning methods, ASR is capable of efficiently exploring dozens of models and their parameter combinations on a given dataset, automatically selecting the optimal configuration, and generating a stable and generalizable prediction model.

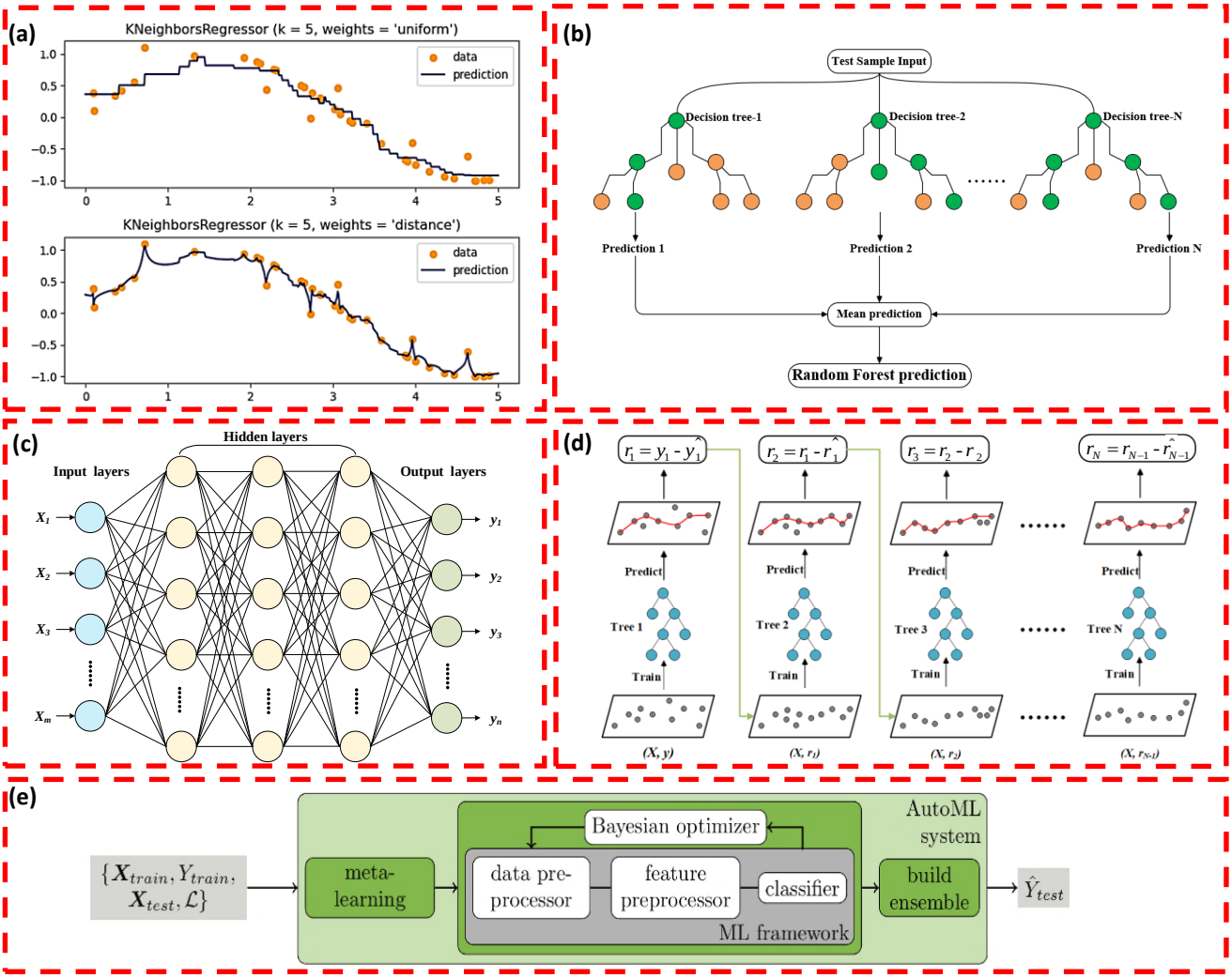


Figure 3. The schematic diagram of the machine learning models: (**a**) KNNs; (**b**) RFs; (**c**) NNs; (**d**) GBR; (**e**) ASR [21].

3. Results and Discussions

3.1. Results of the FEA

Figure 4 presents the stress distribution diagram of the maximum principal stress of metal pressure-bearing components under working conditions with an internal pressure of 16.7 MPa and a temperature of 541 °C at full load. The maximum stress of the MSPT appears at the transition position between the main pipe and the branch pipe, with a

value of approximately 75.4 MPa. The stress concentration area of the DDJ is located at the connection position between the steam drum and the downcomer, with a maximum value of approximately 64.8 MPa. The stress concentration area of the HL is located at the transition position between the header and the branch pipe as well as the inner surface of the orifice bridge, with a maximum principal stress of approximately 78.2 MPa. These stress concentration areas are probably the main parts where cracks or even fractures may occur in various complex pressure-bearing components. The main reason is that the geometric shape change at the connection part between the main pipe and the branch pipe could lead to the accumulation of thermal and residual stresses generated during the welding process in these regions. Additionally, loading conditions such as internal pressure and external forces can lead to the weld seam area being acted on by the load in different directions, thereby causing stress concentration in these areas. Therefore, the locations of the maximum stress points in these areas can be regarded as the dangerous points of the metal pressure-bearing components and be adopted as the object for subsequent machine learning.

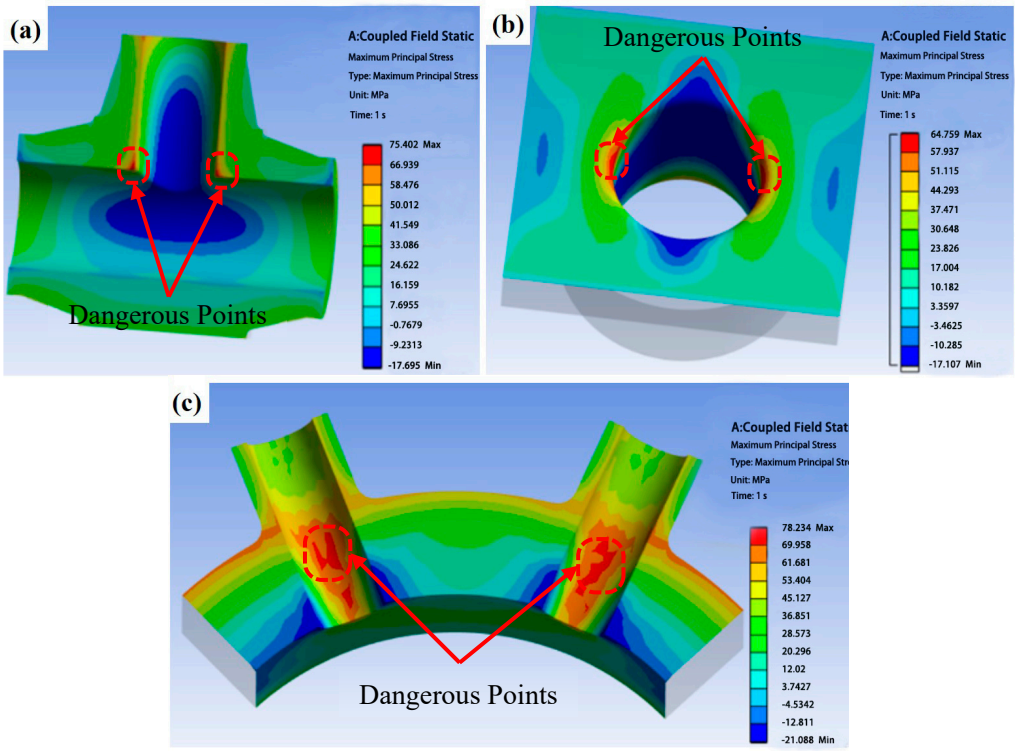


Figure 4. Stress distribution cloud of studied metal pressure-bearing components: (**a**) the MSPT; (**b**) the DDJ; (**c**) the HL.

The stress concentration mechanisms observed in this study are consistent with the results of other research. For instance, Wang et al. [22] analyzed the stress concentration in butt welds with variable wall thickness in spanning pipelines under additional loads, concluding that the weld region serves as a stress-critical zone due to geometric stress accumulation. Similarly, Wang et al. [23] conducted a failure analysis of stress corrosion cracking in the welded structures of aluminum alloy metro body traction beams, emphasizing the influence of geometric stress and residual stress on failure. Moreover, Li et al. [24] investigated the welding residual stress in dissimilar metal butt-welded joints, revealing that the combination of residual stress and geometric transitions is the primary factor contributing to stress concentration.

While these studies provide valuable insights into stress concentration mechanisms and propose structural optimization measures, they primarily focus on static conditions or

simplified working loads, without considering the dynamic variations of stress concentration under actual operating conditions. These variations, influenced by internal pressure, temperature fluctuations, and complex loadings, may result in significant stress fluctuations in critical regions during service. To address this issue, the present study adopts machine learning techniques to evaluate and predict the stress magnitudes in critical areas of pressure-bearing components under real working conditions.

Figure 5 depicts the variation curves of the stress at the dangerous points of each complex pressure-bearing component with temperature and internal pressure under the startup condition (obtained from the FEA calculations), along with the projections of the curves on each plane. The stress of the dangerous points of the MSPT increases linearly with temperature and as a power function with the internal pressure. The values of dangerous points for the DDJ and the HL bridge increase exponentially with temperature and linearly with the internal pressure. Under the combined influence of temperature and internal pressure, the stress-rising tendencies at the dangerous points of the MSPT and the DDJ are relatively homogeneous. However, the initial rising tendency of the stress at the dangerous point of the HL is relatively slow. At the temperature of 350 °C and the pressure of 4 MPa, the maximum stress is only about 20 MPa. The stress increases slowly with the increase of the temperature and pressure initially. However, the increasing rate of the stress would accelerate when the temperature surpasses 400 °C and the pressure surpasses 6 MPa. Additionally, it could be observed that the stress of the dangerous points is smaller than the yield stress, suggesting the elastic deformation of the components, which is further verified by FEA. Therefore, the deformation is recoverable and does not exceed the permissible design tolerances during the startup condition. However, any excessive deformation should be followed further during the long-term service, especially the deformation induced by the accumulative damage over time.

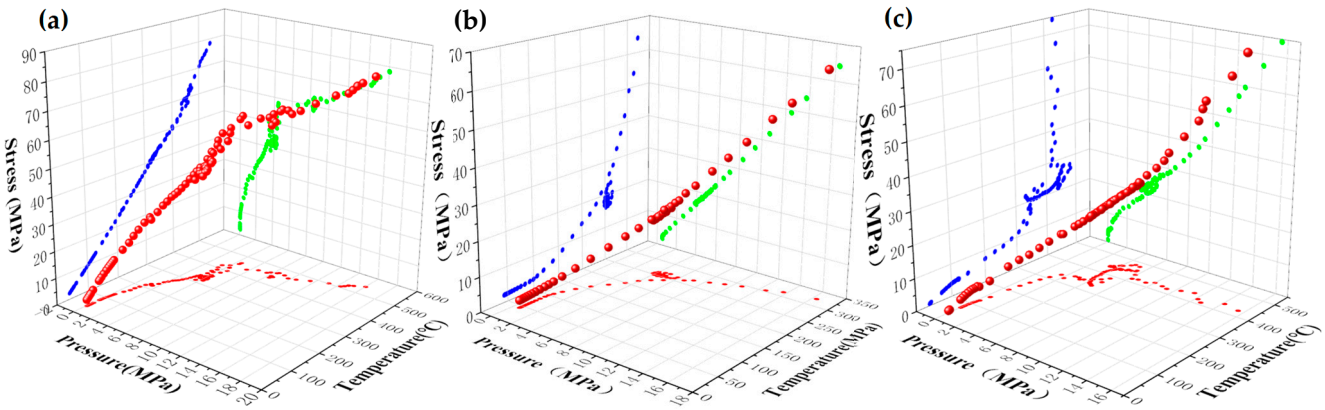


Figure 5. The variation curves of the stress at the dangerous points of various complex metal pressure-bearing components under the startup condition versus the temperature and internal pressure: (**a**) the MSPT; (**b**) the DDJ; (**c**) the HL.

3.2. Stress Prediction by Machine Learning

Apparently, the internal pressure significantly influences the maximum principal stress of the component, but its irregular change would complex the fitting of the maximum principal stress through a simple mathematical model. The large consumption of time and resources of FEA suggests that FEA is not suitable for the real-time analysis of stress during emergency events. Therefore, the machine learning method was performed for the stress prediction of the components.

At first, the stress at different temperatures and pressure of the startup parameters was calculated by FEA to obtain sufficient data for machine learning. The variation range of the

temperature and the internal pressure for studying was 40~529 °C and 0.07~16 MPa for the MSPT, while 42~324 °C and 0.53~16.7 MPa for the DDJ, 37~426 °C and 0.028~15.5 MPa for the HL. The value-taking interval for the FEA parametric calculation was 1 min, and 500 sets of original sample data were finally obtained. The startup parameters in the typical sample library are presented in Table 2.

Table 2. The parameters for startup conditions.

No.	MSPT			DDJ			HL		
	Temperature (°C)	Internal Pressure (MPa)	Stress (MPa)	Temperature (°C)	Internal Pressure (MPa)	Stress (MPa)	Temperature (°C)	Internal Pressure (MPa)	Stress (MPa)
1	40.6	0.06	2.37	43.7	0.54	2.35	37.6	0.02	0.71
2	40.7	0.07	2.38	43.6	0.54	2.54	37.7	0.02	0.73
3	41.1	0.07	2.42	43.8	0.57	2.56	37.8	0.03	0.73
⋮	⋮	⋮	⋮	⋮	⋮	⋮	⋮	⋮	⋮
529	532.6	15.6	76.67	326.2	16.7	70.06	434.2	15.3	72.61

Subsequently, the sample data were subjected to preprocessing. The input parameters were designated as internal pressure and operating temperature, while the output parameter was the stress value at the perilous point. To ensure the accuracy and convergence of the prediction models, the sample magnitude had to be maintained consistently. Thus, the input and output data were normalized [25] with the data scaled within the range of [−1~1]. To eliminate contingency and guarantee the universality of various models, the sample data were randomly shuffled prior to training, allowing the model to learn and validate under a more random and diverse data distribution, unaffected by a specific sequence. Meanwhile, 80% of the shuffled sample data was randomly selected as the training set, and the remaining 20% was utilized as the test set to evaluate the model's generalization ability in different datasets more comprehensively.

The language employed in machine learning was Python, and the platform selected was Google Colaboratory. This platform does not necessitate the configuration of a cumbersome development environment and offers free GPU and TPU support, facilitating users in conducting machine learning and data analysis. In the training period, the scaled data after normalization were utilized to train the prediction model. In the testing stage, the scaled data of the stress prediction results at the dangerous points were acquired first, and then the data restoration of these predicted results was carried out. Finally, the restored predicted stress values were compared with the results of the FEA calculation.

After carrying out learning and training on the aforementioned start-up samples, the reserved test set was utilized to verify the accuracy of the learning models. Figure 6 presents the radar diagram of the evaluation indicators for different models at the dangerous points of the MSPT under the startup condition on the training set. It is evident from the results that significant discrepancies exist in the fitting capabilities and predictive accuracies among different models. Specifically, the determination coefficients of the KNNs, RFs, and GBR models are all significantly lower than those of the NNs and ASR models. This relatively low determination coefficient indicates that the aforementioned three models fail to precisely capture the variation patterns of the principal stresses at the dangerous points under the start-up conditions, and their fitting performances are unsatisfactory. Moreover, in terms of the error indicators, the mean absolute error (MAE) and mean square error (MSE) of the KNNs, RFs, and GBR models are markedly higher than those of the NNs and ASR models, and their prediction accuracy is relatively low.

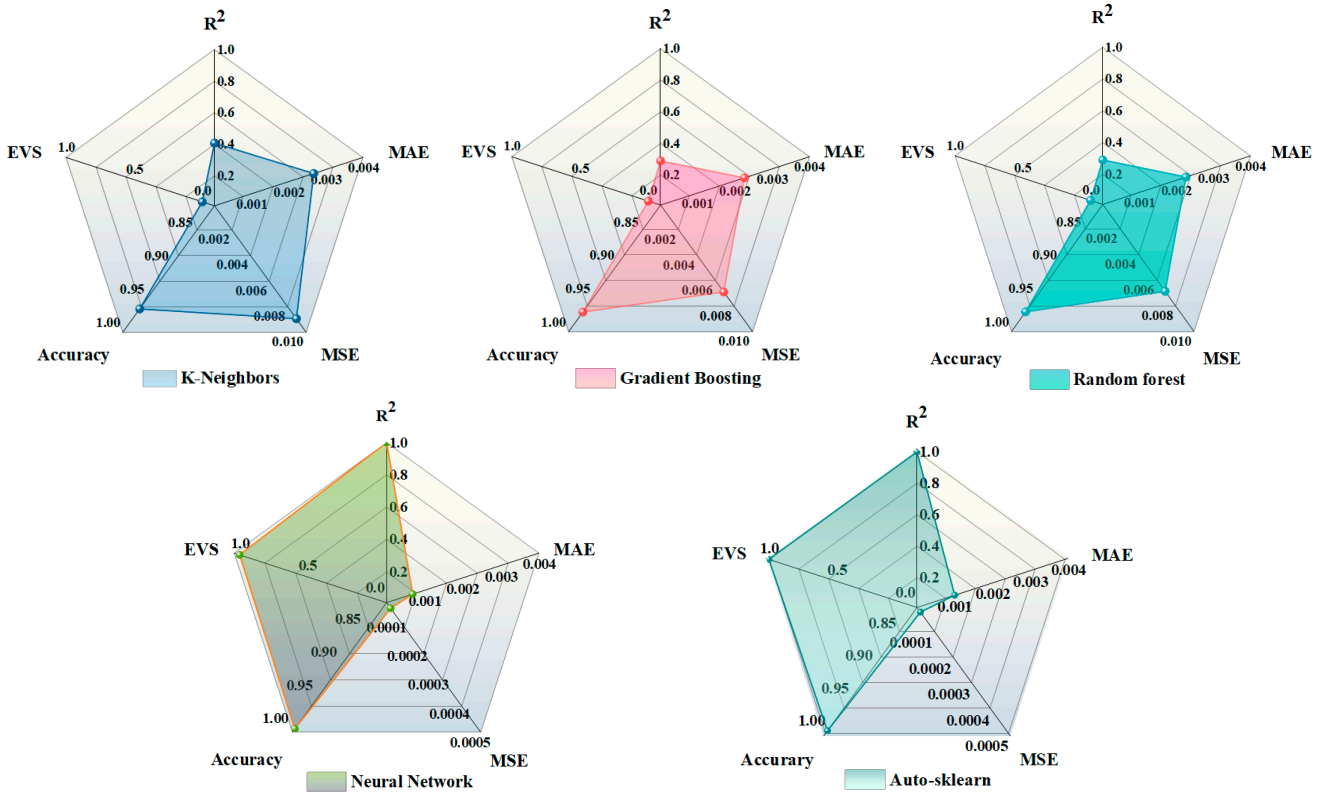


Figure 6. Performance comparison of different machine learning models.

In addition, Figure 7 shows the bar chart of the validation results on the test set. The prediction outcomes of the KNNs, RFs, and GBR models are highly similar and nearly converge to the same level. The fundamental reason for this phenomenon lies in the fact that the time interval between adjacent groups in the original sample data is relatively short, and the stress value at a certain moment at the dangerous point is highly dependent on the stress value at the previous moment. This results in an overly high similarity of features among adjacent group samples, thereby making it challenging for the three models to accurately model the complex temporal dependency relationships. Consequently, these models exhibit significant limitations in predicting the maximum principal stress of special-shaped pressure-bearing components under startup conditions.

In contrast, the NNs and ASR models showcase remarkable performance in addressing complex nonlinear relationships and temporal dependency matters. Not only do they possess a satisfactory fitting effect on the training set, but they also maintain a relatively low prediction error on the test set, along with higher prediction accuracy. As a consequence, the NNs and ASR models were selected subsequently for predicting the maximum principal stress values at the dangerous points of the DDJ and HL components. The specific structure and performance parameters of the neural network are presented in Table 3. To validate the actual prediction accuracy of these two models, 10 sets of data of different times, temperatures, and internal pressures were randomly selected, and the predictions were conducted through ANSYS calculation and machine learning. The calculation results and the prediction accuracy of the two models are listed in Tables 4 and 5, respectively. The comparison results between the predicted values and the random samples are depicted in Figure 8.

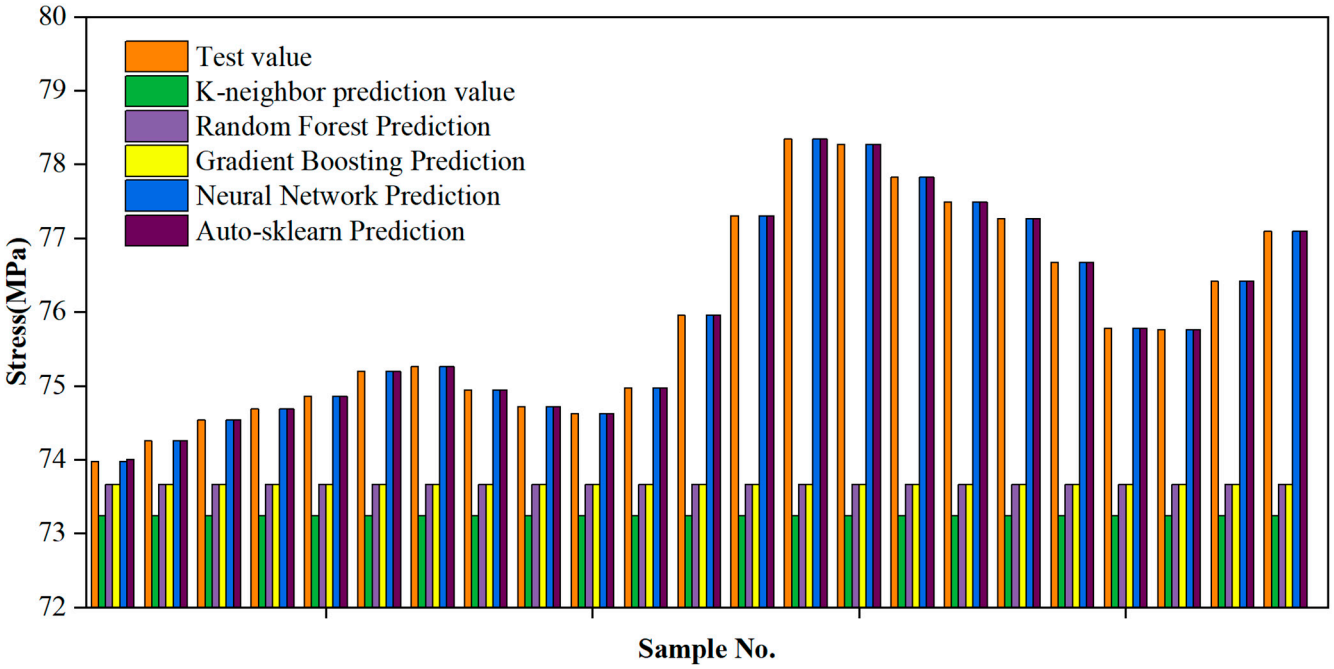


Figure 7. Comparison of the predicted results by using different machine learning models.

Table 3. The structure and performance parameters of artificial neural networks.

Performance Parameters	Value	Number of Neurons	Activation Function	Type
Input dimension	2	-	-	-
Output layer	1	1	Linear	-
Hidden layer	5	256-128-64-32-16	ReLU	-
Optimizer	-	-	-	Adam
Learning rate	0.1	-	-	-
Loss function	-	-	-	MSE
Index	-	-	-	RMSE
Number of Iterations	1000	-	-	-

Table 4. Validation of prediction results with random sample data.

No.	Temperature (°C)	Internal Pressure (MPa)	Results of FEA (MPa)			Prediction Results of Neural Networks (MPa)			Prediction Results of Auto-Sklearn (MPa)		
			MSPT	DDJ	HL	MSPT	DDJ	HL	MSPT	DDJ	HL
1	80	0.09	7.251	1.920	2.663	6.065	2.537	2.722	8.413	1.830	3.118
2	120	0.3	12.379	2.994	3.846	13.431	3.306	4.136	12.764	3.368	4.328
3	150	0.5	16.262	3.880	5.043	18.734	3.525	5.457	18.372	5.485	6.981
4	350	5	44.873	21.617	23.553	45.383	23.463	22.933	46.137	22.396	23.621
5	400	7	52.780	28.907	31.763	53.024	30.165	27.677	52.779	30.281	30.329
6	420	9	56.975	35.972	40.151	57.403	34.107	40.306	56.765	36.401	39.948
7	450	10	61.547	39.786	44.867	63.484	41.006	48.552	63.417	39.877	46.079
8	470	11	64.882	43.547	49.761	66.828	43.438	54.110	64.810	43.753	50.307
9	500	13	70.314	51.368	59.730	74.411	49.793	63.468	70.514	50.126	59.427
10	540	15	76.984	59.208	69.519	79.916	58.574	71.484	76.399	58.516	70.280

Table 5. Prediction accuracy and fitting degree (R2) of random samples.

Model	MSPT		DDJ		HL	
	Accuracy	R2	Accuracy	R2	Accuracy	R2
NNs	94.181%	0.9980	92.276%	0.9981	94.011%	0.9869
ASR	96.050%	0.9928	92.762%	0.9965	92.124%	0.9983

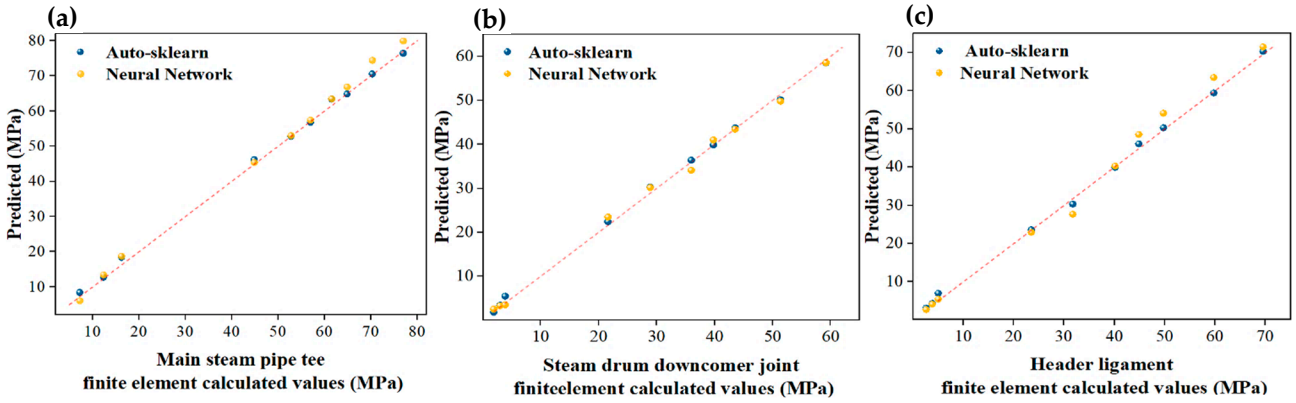


Figure 8. Comparison between predicted values and calculation results by finite element method: (**a**) the MSPT; (**b**) the DDJ; (**c**) the HL.

From Table 4 and Figure 8, it is evident that the NN and ASR models offer highly similar predictions regarding the principal stresses of the MSPT, DDJ and HL components. Figure 8 presents the comparison between the predictions of the two models and the FEA calculation values in a random sample. Both models can accurately capture the stress variation characteristics at low temperatures and low pressure, with the predicted values being in substantial agreement with the FEA results. Nevertheless, at high temperatures and high pressure, the ASR model demonstrates superior fitting ability and has smaller prediction errors. For instance, the predicted values of the NNs and ASR models are highly in line with the finite element calculation results at a temperature of 80 °C and internal pressure of 0.09 MPa (Group 1 in Table 4), suggesting that both models can precisely capture the variation of principal stresses under low-temperature and low-pressure scenario circumstances. Nevertheless, the performance of the models starts to differ in high-temperature and high-pressure conditions (such as Group 10 in Table 4). For the complex condition with a temperature of 540 °C and an internal pressure of 15 MPa, the ASR model can still accurately approximate the finite element results, while the predicted values of the NN model for some components (such as the DDJ) are slightly lower than the finite element calculation values. This might be due to the more complex nonlinear characteristics of the stress distribution in high-temperature and high-pressure conditions, causing the NN model to present a certain degree of underfitting.

From the performance of various components, the predicted errors of the MSPT and the HL are relatively small, and their stress distribution patterns are rather simple and stable, facilitating their learning by the model. Particularly, the predicted results of the MSPT, as depicted in Figure 8a, the predicted values of the two models almost completely coincide with the finite element results, suggesting that the stress change characteristics of this component are highly suitable for machine learning modeling. In contrast, the predicted error of the boiler DDJ is slightly larger. Especially as can be observed in Figure 8b, the stress distribution of this component is significantly influenced by complex loads and multi-field coupling, which poses more challenges to the models' prediction. Nonetheless, the ASR model still exhibits higher prediction accuracy in most cases, and its ability to fit complex stress features is superior to that of the NN model.

From the accuracy analysis in Table 5, the ASR model has higher prediction accuracy than the neural network model for all three components. The prediction accuracy of the MSPT reaches 96.05%, which is nearly 2 percentage points higher than that of the NN model. This further indicates that the ASR model has more advantages in capturing the stress distribution pattern of this component. Additionally, although the difference in prediction accuracy between the two models is not significant for the DDJ and HL, the overall performance of the ASR model is more stable. Especially in complex working conditions, its ability to capture the main stress demonstrates stronger robustness.

Based on the comprehensive analysis of Table 4, Table 5 and Figure 8, it can be observed that the ASR model slightly outperforms the NN model in terms of prediction accuracy and stability, particularly with a more prominent performance under complex working conditions. Although the NN model has certain errors in some high-temperature and high-pressure conditions, its efficient training speed and decent predictive capability still render significant value in practical engineering applications. For the boiler DDJ, a component with a complex stress distribution, future studies can further enhance the predictive performance of the machine learning model by improving the model structure or introducing auxiliary variables related to multi-field coupling characteristics. In addition, it should be observed that the completion time for all the abovementioned predictions was less than 2 min. Therefore, the machine learning approach exhibits a significantly superior calculation speed for the maximum principal stress in the internal dangerous areas of special-shaped metal pressure-bearing components compared to the finite element method, and the accuracy of the predicted values is high, which can satisfy the requirements for online stress prediction of special-shaped metal pressure-bearing components in thermal power plants in engineering practice.

However, it should be mentioned that there are certain limitations in this study that warrant further attention in future research:

Firstly, this study does not address cumulative damage and thermal fatigue behavior. In real-world working conditions, stress fluctuations in pressure-bearing components not only cause changes in the peak stress of critical regions but also lead to the accumulation of thermal fatigue damage over long-term operation, significantly reducing the service life of the components [26]. Future work could incorporate cumulative damage models and thermal fatigue analysis into the stress prediction framework to provide a more comprehensive assessment of component lifespan.

Second, this study does not delve into the crack initiation and propagation behavior in critical regions. Crack formation and growth are key factors affecting the structural integrity of pressure-bearing components [27]. Under alternating high-temperature and high-pressure loads, the rate and path of crack propagation could be significantly influenced by the complex stress field. Future studies should integrate fracture mechanics theories to simulate and predict crack growth behavior in critical regions, providing more comprehensive support for the reliability assessment of components.

Finally, although the proposed FEA-machine learning method achieves high prediction accuracy, the applicability and robustness of the model are somewhat limited by the quality of the sample data. Future research could focus on expanding the dataset under various operating conditions, optimizing feature extraction methods, and improving the architecture of the machine learning models to further enhance prediction accuracy [28]. In addition, the application of this method is currently confined to certain pressure-bearing components. Future efforts could explore its extension to other critical pressure-bearing components in thermal power plants, such as steam pipelines, super-heaters, and re-heaters, to further validate its generalizability and applicability.

4. Conclusions

In this study, FEA was carried out on the typical special-shaped metal pressure-bearing components of the boiler in thermal power plants, and the dangerous areas within the components were identified. The machine learning method was then adopted to predict the stress in the dangerous areas of the special-shaped components, providing a new method for the stress prediction of the special-shaped pressure-bearing components.

The stress prediction method for the dangerous areas of special-shaped metal pressure-bearing components in the boilers of thermal power plants based on the combination of finite element and machine learning proposed in this study can rapidly predict the stress values at the dangerous points of the components under the startup state. The calculation speed of this method is significantly superior to the finite element method, and the predicted values have a high degree of consistency with the finite element simulation results, making it applicable to the online stress monitoring and analysis of large and complex structural metal components.

Future research will focus on cumulative damage and thermal fatigue analysis, as well as the prediction of crack initiation and propagation behavior. These efforts will provide more comprehensive and reliable solutions for the safety assessment and lifespan management of pressure-bearing components in thermal power plant boilers.

Author Contributions: Conceptualization, S.W. and H.L.; methodology, J.W. and Y.M.; software, R.S.; validation, S.W., C.Y. and H.L.; formal analysis, J.W.; investigation, J.W. and Y.M.; resources, S.W. and H.L.; writing—original draft preparation, S.W., Y.M. and J.W.; writing—review and editing, H.L.; supervision, H.L.; funding acquisition, S.W. and H.L. All authors have read and agreed to the published version of the manuscript.

Funding: This research was funded by the Technology Project of State Grid Corporation of China, grant number 0FW-221141-JS.

Data Availability Statement: The original contributions presented in the study are included in the article, further inquiries can be directed to the corresponding author.

Conflicts of Interest: Authors S.W., R.S. and C.Y. were employed by the company Jiangsu Frontier Electric Power Technology Co., Ltd. The remaining authors declare that the research was conducted in the absence of any commercial or financial relationships that could be construed as a potential conflict of interest.

References

1. Pivdiablyk, I.; Di Goh, Z.; Chye, L.K. Residual Creep Life Assessment of High-Temperature Components in Power Industry. *Sensors* **2023**, *23*, 2163. [CrossRef] [PubMed]
2. Bhiogade, D.S. Ultra Supercritical Thermal Power Plant Material Advancements: A Review. *J. Alloys Metall. Syst.* **2023**, *3*, 100024. [CrossRef]
3. Duda, P. Heat Transfer Coefficient Distribution—a Review of Calculation Methods. *Energies* **2023**, *16*, 3683. [CrossRef]
4. Huang, S.; Yang, Y.; Huang, B. Health Status Analysis and Optimization of Load Dispatch for Power Plant Boiler. *J. Comput. Inf. Sci. Eng.* **2021**, *21*, 011004. [CrossRef]
5. Liu, W.; Li, S.; Park, H.S. Eighty Years of the Finite Element Method: Birth, Evolution, and Future. *Arch. Comput. Methods Eng.* **2022**, *29*, 4431–4453. [CrossRef]
6. Dogan, B.; Ainsworth, R. Defect Assessment Procedure for Low to High Temperature Range. In Proceedings of the ASME 2003 Pressure Vessels and Piping Conference, Cleveland, OH, USA, 20–24 July 2003.
7. Jawad, M.H. *Stress in Asme Pressure Vessels, Boilers, and Nuclear Components*; John Wiley & Sons: Hoboken, NJ, USA, 2017.
8. Hazizi, K.; Ghaleeh, M. Design and Analysis of a Typical Vertical Pressure Vessel Using Asme Code and Fea Technique. *Designs* **2023**, *7*, 78. [CrossRef]
9. Taraphdar, P.K.; Kumar, R.; Pandey, C. Significance of Finite Element Models and Solid-State Phase Transformation on the Evaluation of Weld Induced Residual Stresses. *Met. Mater. Int.* **2021**, *27*, 3478–3492. [CrossRef]

10. Abdelouahed, E.; Mokhtari, M.; Benzaama, H. Finite Element Analysis of the Thermo-Mechanical Behavior of Composite Pipe Elbows under Bending and Pressure Loading. *Frat. Integrità Strutt.* **2019**, *13*, 698–713. [CrossRef]
11. Kalu, I.E.; Inglis, H.M.; Kok, S. Failure Assessment Methodology for Boiler Tubes with Localized External Erosion Defects. *Int. J. Press. Vessel. Pip.* **2020**, *188*, 104190. [CrossRef]
12. Nahal, M.; Khelif, R. A Finite Element Model for Estimating Time-Dependent Reliability of a Corroded Pipeline Elbow. *Int. J. Struct. Integr.* **2021**, *12*, 306–321. [CrossRef]
13. Taler, J.; Węglowski, B.; Taler, D. Determination of Start-up Curves for a Boiler with Natural Circulation Based on the Analysis of Stress Distribution in Critical Pressure Components. *Energy* **2015**, *92*, 153–159. [CrossRef]
14. Bolandi, H.; Li, X.; Salem, T. Deep Learning Paradigm for Prediction of Stress Distribution in Damaged Structural Components with Stress Concentrations. *Adv. Eng. Softw.* **2022**, *173*, 103240. [CrossRef]
15. Croom, B.P.; Berkson, M.; Mueller, R.K. Deep Learning Prediction of Stress Fields in Additively Manufactured Metals with Intricate Defect Networks. *Mech. Mater.* **2022**, *165*, 104191. [CrossRef]
16. Xiang, K.; Qin, L.; Zhao, Y.; Huang, S.; Du, W.; Boller, E.; Rack, A.; Li, M.; Mi, J. Operando Study of the Dynamic Evolution of Multiple Fe-Rich Intermetallics of an Al Recycled Alloy in Solidification by Synchrotron X-Ray and Machine Learning. *Acta Mater.* **2024**, *279*, 120267. [CrossRef]
17. Mathew, J.; Griffin, J.; Alamaniotis, M. Prediction of Welding Residual Stresses Using Machine Learning: Comparison between Neural Networks and Neuro-Fuzzy Systems. *Appl. Soft Comput.* **2018**, *70*, 131–146. [CrossRef]
18. *GB/T 16507.2-2022*; Water Tube Boilers Part 2: Materials. Standards Press of China: Beijing, China, 2022.
19. Wei, J.; Chu, X.; Sun, X.Y.; Xu, K.; Deng, H.X.; Chen, J.; Wei, Z.; Lei, M. Machine Learning in Materials Science. *InfoMat* **2019**, *1*, 338–358. [CrossRef]
20. Feurer, M.; Eggensperger, K.; Falkner, S.; Lindauer, M.; Hutter, F. Auto-Sklearn 2.0: Hands-Free Automl Via Meta-Learning. *J. Mach. Learn. Res.* **2022**, *23*, 1–61.
21. Feurer, M.; Klein, A.; Eggensperger, K.; Springenberg, J.; Blum, M.; Hutter, F. Efficient and Robust Automated Machine Learning. *Adv. Neural Inf. Process. Syst.* **2015**, *28*, 1–6.
22. Wang, L.; Tang, Y.; Ma, T.; Zhong, J.; Li, Z.; Zhang, Y.; Xuan, H. Stress Concentration Analysis of Butt Welds with Variable Wall Thickness of Spanning Pipelines Caused by Additional Loads. *Int. J. Press. Vessel. Pip.* **2020**, *182*, 104075. [CrossRef]
23. Wang, C.; Zhu, T.; Yang, B.; Xiao, S.; Yang, G. Failure Analysis of Stress Corrosion Cracking in Welded Structures of Aluminum Alloy Metro Body Traction Beam in Service. *Eng. Fail. Anal.* **2024**, *163*, 108564. [CrossRef]
24. Li, S.; Li, J.; Sun, G.; Deng, D. Modeling of Welding Residual Stress in a Dissimilar Metal Butt-Welded Joint between P92 Ferritic Steel and Sus304 Austenitic Stainless Steel. *J. Mater. Res. Technol.* **2023**, *23*, 4938–4954. [CrossRef]
25. Werner de Vargas, V.; Schneider Aranda, J.A.; dos Santos Costa, R.; da Silva Pereira, P.R.; Victória Barbosa, J.L. Imbalanced Data Preprocessing Techniques for Machine Learning: A Systematic Mapping Study. *Knowl. Inf. Syst.* **2023**, *65*, 31–57. [CrossRef] [PubMed]
26. Liu, F.; Song, C.; Pan, W.; Wang, G.; Zhang, H.; Lei, Y. Thermal Fatigue Analysis of District Heating Pipeline under Variable Frequency Regulation of Circulating Water Pump. *Appl. Therm. Eng.* **2024**, *242*, 122535. [CrossRef]
27. Fan, Y.; Shuai, Y.; Shuai, J.; Zhang, T.; Zhang, Y.; Shi, L.; Shan, K. The Effect of Pipeline Root Weld Microstructure on Crack Growth Behaviour. *Eng. Fail. Anal.* **2024**, *161*, 108265. [CrossRef]
28. Prada Parra, D.; Ferreira, G.R.B.; Díaz, J.G.; Gheorghe de Castro Ribeiro, M.; Braga, A.M.B. Supervised Machine Learning Models for Mechanical Properties Prediction in Additively Manufactured Composites. *Appl. Sci.* **2024**, *14*, 7009. [CrossRef]

Disclaimer/Publisher's Note: The statements, opinions and data contained in all publications are solely those of the individual author(s) and contributor(s) and not of MDPI and/or the editor(s). MDPI and/or the editor(s) disclaim responsibility for any injury to people or property resulting from any ideas, methods, instructions or products referred to in the content.